

***Ab initio* study on oxidized silicon clusters and silicon nanocrystals embedded in SiO₂: Beyond the quantum confinement effect**

Marcello Luppi^{1,*} and Stefano Ossicini²

¹*INFN National Center on nanoStructures and bioSystems at Surfaces (S³), and Dipartimento di Fisica, Università di Modena e Reggio Emilia, I-41100 Modena, Italy*

²*INFN National Center on nanoStructures and bioSystems at Surfaces (S³), and Dipartimento di Scienze e Metodi dell'Ingegneria, Università di Modena e Reggio Emilia, I-42100 Reggio Emilia, Italy*

(Received 25 February 2004; revised manuscript received 29 September 2004; published 27 January 2005)

Density-functional theory calculations have been carried out in order to study the structural, electronic, and optical properties of oxidized silicon clusters and silicon nanocrystals embedded in SiO₂. For the isolated clusters, different Si/O bonding geometries and various levels of oxidation have been investigated, checking also the dependence of the results on the structure size. We provide strong evidences that not only the quantum confinement effect but also the chemistry at the interface has to be taken into account in order to understand the physical properties of these systems. In particular we show how the multiple presence of silanone-like Si=O bonds can be a reliable model for explaining the photoluminescence redshift observed in oxidized porous silicon samples and it can be used as possible explanation also for the unexpected large photoluminescence bandwidth in single oxidized Si quantum dots. For the silicon nanocrystals embedded in a SiO₂ matrix, the electronic and optical properties are discussed in detail. The strong interplay between the nanocrystal and the surrounding host environment and the active role of the interface region between them is pointed out, in very good agreement with the experimental results.

DOI: 10.1103/PhysRevB.71.035340

PACS number(s): 73.22.-f, 78.67.Bf, 73.20.At

I. INTRODUCTION

Silicon microelectronics devices have revolutionized our life in the second half of the last century. Integration and economy of scale are the two key ingredients for the silicon technological success. Silicon has a band gap of 1.12 eV that is ideal for room-temperature operation and an oxide that allows the processing flexibility to place today more than 10⁸ transistors on a single chip. The extreme integration levels reached by silicon microelectronics industry have permitted high-speed performance and unprecedented interconnection levels. The present interconnection degree is sufficient to cause interconnect propagation delays, overheating, and information latency between single devices. To overcome this bottleneck, photonic materials, in which light can be generated, guided, modulated, amplified, and detected, need to be integrated with standard electronics circuits to combine the information processing capabilities of electronic data transfer and the speed of light. In particular, chip to chip or even intrachip optical communications all require the development of efficient optical functions and their integration with state-of-the-art electronic functions.¹

Silicon is the desired material, because silicon optoelectronics would open the door to faster data transfer and higher integration densities at very low cost. Silicon microphotronics has boomed these last years. Almost all the various photonic devices have been demonstrated,¹⁻³ the main limitation of silicon photonics remains the lack of any practical Si-based light sources. Several attempts have been employed to engineer luminescing transitions in an otherwise indirect material.¹ After the initial impulse given by the pioneering work of Canham on photoluminescence (PL) from porous silicon (PS),⁴ nanostructured silicon has received extensive

attention (for review see Refs. 5 and 6). This activity is mainly centered on the possibility of getting relevant optoelectronic properties from nanocrystalline Si. It is generally accepted that the quantum confinement, caused by the restricted (nanometric) size, is essential for the visible light emission in Si nanostructures^{1,5} but some controversial interpretations of the PL properties of low-dimensional Si structures still exist. The question of surface effects, in particular oxidation, has been addressed in the last years. Both theoretical calculations and experimental observations have been applied to investigate the possible active role of the interface on the optoelectronic properties of Si nanostructures. Different models have been proposed: Baierle *et al.*⁷ considered the role of the surface geometry distortion of small hydrogenated silicon cluster in the excited state. Wolkin *et al.*⁸ observed that oxidation introduces defects in the Si-nanocrystal (NC) band gap which pin the transition energy. They claimed the formation of a Si=O double bond as the pinning state. The same conclusion has been reached in Ref. 9 and by us,¹⁰ whereas Vasiliev *et al.*¹¹ have pointed out that similar results can be obtained also for O connecting two Si atoms (single bond) at the Si-NC surface. In Ref. 12, the assistance of Si-O vibrations at the interface has been proposed as the dominant path for recombination. The optical gain observed in Si-NC's formed by ion implantation in SiO₂,¹³ by plasma enhanced chemical vapor deposition (PECVD),¹⁴ and samples prepared by magnetron sputtering¹⁵ is giving a further impulse to these studies. Interface radiative states have been suggested to play a key role in the mechanism of population inversion at the origin of the gain.^{13,14,16}

This paper aims at answering the question of the absorption and photoluminescence origin in silicon nanostructures.

We provide strong evidences that the role of the interface region surrounding the silicon nanostructures have to be carefully taken into account in order to understand the striking optical properties of these systems. Within the framework of the density-functional theory (DFT) we have extensively studied the effects of oxygen on the electronic and optical properties of various types of silicon clusters. Varying the cluster size we have considered different bonding geometries and different levels of oxidation. Moreover, we have performed *ab initio* total-energy calculations on small silicon nanocrystals embedded in a SiO₂ matrix stressing the interplay between the nanocrystal and the surrounding host environment.

The paper is organized as follows. A brief description of the computational methods is given in Sec. II. The study of the isolated Si clusters is presented in Sec. III. First the effects of the different Si/O bond geometries (Sec. III B) are discussed, then the specific case of multiple oxygen passivation with silanone-like Si=O bonds (Sec. III C) is considered. This particular bond has been studied also in view of its role in the initial state of silicon oxidation.¹⁷ The work on Si nanocrystals embedded in SiO₂ is reported in Sec. IV, where the electronic and optical properties are extensively discussed. Finally in Sec. V some conclusions are presented.

II. COMPUTATIONAL METHODS

All calculations have been performed within the framework of the density-functional theory (DFT) with a plane-wave pseudopotential approach. For the study of the isolated nanostructures, two different codes have been used: FHI98MD (Ref. 18) and CASTEP.^{19–21} In the first case the electron-ion interaction has been described via norm-conserving pseudopotentials²² generated following Martins-Troullier prescriptions;²³ in the second case via ultrasoft pseudopotentials.²⁴ Different cutoffs for the wave-function kinetic energy have thus been adopted: 680 eV in FHI98MD and 380 eV in CASTEP. The structural relaxation (SR) has been achieved using indifferently both codes, while the optoelectronic properties at relaxed geometry have been determined with CASTEP. For the embedded nanocrystals case we have used CASTEP only, with special pseudopotentials suitable for high-performance solid-state calculations²¹ and a kinetic energy cutoff of 260 eV.

The relaxed geometry has been obtained within the local-density approximation (LDA) for the isolated clusters, while for the embedded nanocrystals within the generalized gradient approximation with the PBE exchange and correlation (XC) functional. In all the cases one special k point (Γ) has been used for the Brillouin zone (BZ) sampling. During the relaxation procedure all the atoms (in the isolated and embedded systems) and the cell parameters (in the embedded systems) have been left free to relax. The tolerance for the force on atoms has been set to 0.05 eV/Å, a compromise between good accuracy and computational speed. For the electronic minimization we have used a density mixing scheme with conjugate gradient (CG) Pulay solver;²¹ for the internal coordinates optimization a Broyden-Fletcher-Goldfarb-Shanno (BFGS) scheme.²¹

TABLE I. List of all the studied clusters, classified by the type of surface passivation (rows) and by the core size (columns). “Full-H” stands for a passivation by H atoms only; “Si–O–Si” by H atoms plus O in the backbond geometry; “Si=O” by H atoms plus O in the double-bond geometry; and “Si–O–Si+Si=O” by H atoms plus O both in the back- and double-bond geometry.

Bond/size	0.5 nm	0.7 nm	1.0 nm
full-H	Si ₁₀ H ₁₆	Si ₁₄ H ₂₀ Si ₁₂ H ₁₆	Si ₃₅ H ₃₆
Si–O–Si	Si ₉ H ₁₄ –O	Si ₁₄ H ₂₀ –O ₂ Si ₁₃ H ₁₈ –O Si ₁₂ H ₁₆ –O ₂	Si ₃₄ H ₃₄ –O
Si=O	Si ₁₀ H ₁₄ =O Si ₁₀ H ₁₂ =O ₂ Si ₁₀ H ₁₀ =O ₃ Si ₁₀ H ₈ =O ₄ Si ₁₀ H ₆ =O ₅ Si ₁₀ H ₄ =O ₆	Si ₁₄ H ₁₈ =O Si ₁₄ H ₁₆ =O ₂ Si ₁₄ H ₈ =O ₆ Si ₁₃ H ₁₈ =O Si ₁₂ H ₁₆ =O ₂	Si ₃₅ H ₃₄ =O Si ₃₅ H ₃₂ =O ₂ Si ₃₅ H ₃₀ =O ₃ Si ₃₅ H ₂₈ =O ₄ Si ₃₅ H ₂₄ =O ₆
Si–O–Si +Si=O		Si ₁₃ H ₁₆ –O=O	

At relaxed geometry the electronic properties in terms of band-structure/energy levels, total density of states (TDOS), and orbital spatial distribution have been determined using the same level of theory adopted during the SR. The optical properties have been instead calculated within LDA with a band-by-band scheme and for the embedded structures the calculations were performed on different k points.²⁵ The absorption spectra have been obtained considering only direct (same k point) interband (between valence and conduction bands) transitions, with no phonon assistance and with the electric-field vectors taken as a fully isotropic average. No self-energy corrections, local-field, and excitonic effects have been included. The choice of displaying the optical results through the absorption spectra (derived from the imaginary part of the dielectric function²¹) is due to the possibility of an easier comparison with the experimental measurements.

For the isolated systems, because our method employs three-dimensional periodic boundary conditions, the clusters were placed at the center of a simple-cubic supercell of vacuum in order to ensure a complete isolation. Various tests have been performed considering different supercell side lengths for each cluster size. The final side lengths have been set between 1.4 and 1.8 nm in order to ensure, for all the cluster sizes, a minimum distance of 0.8 nm between the nearest atoms of the repeated supercells. In order to test our setting band-structure calculations have been carried out for some systems at relaxed geometry. The flat behavior of the electronic bands for the entire valence band (VB) and around the bottom edge of the conduction band (CB) proves the achievement of a good confinement.

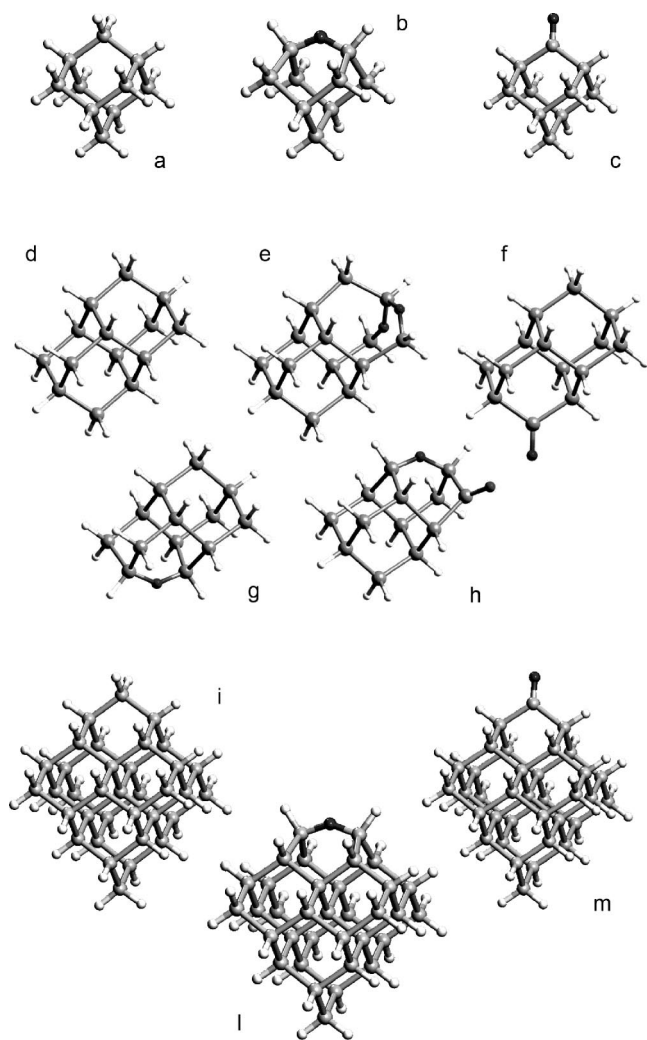


FIG. 1. Stick and ball representation of the final relaxed structures of some of the studied systems. The grey balls stand for the Si atoms, the black ones for the oxygen, and the small white ones for the hydrogen. (a) $\text{Si}_{10}\text{H}_{16}$; (b) $\text{Si}_9\text{H}_{14}\text{-O}$; (c) $\text{Si}_{10}\text{H}_{14}\text{=O}$; (d) $\text{Si}_{14}\text{H}_{20}$; (e) $\text{Si}_{14}\text{H}_{20}\text{-O}_2$; (f) $\text{Si}_{14}\text{H}_{18}\text{=O}$; (g) $\text{Si}_{13}\text{H}_{18}\text{-O}$; (h) $\text{Si}_{13}\text{H}_{16}\text{-O=O}$; (i) $\text{Si}_{35}\text{H}_{36}$; (l) $\text{Si}_{34}\text{H}_{32}\text{-O}$; (m) $\text{Si}_{35}\text{H}_{34}\text{=O}$.

III. ISOLATED CLUSTERS

Silicon nanoclusters with a passivated surface are used as the natural trial model for theoretical simulations on silicon-based light emitting materials, such as porous silicon (PS) or Si-NC's. In a Si zero-dimensional (0D) system, in fact, the strong quantum confinement can increase the optical infrared gap of bulk Si and consequently shift the optical transition energies towards the visible range.^{26,27} This, for many years, has been considered the main explanation of the visible photoluminescence (PL) from PS. In the literature most first-principle calculations and empirical simulations have used hydrogen as passivating agent for the dots surface.^{7,28-37} On the other hand, porous and nanocrystalline silicon samples are obtained with a great variety of surface conditions. The above-mentioned theoretical studies are in good agreement with optical absorption measurements on hydrogen-passivated silicon clusters,³⁸ but experiments performed on

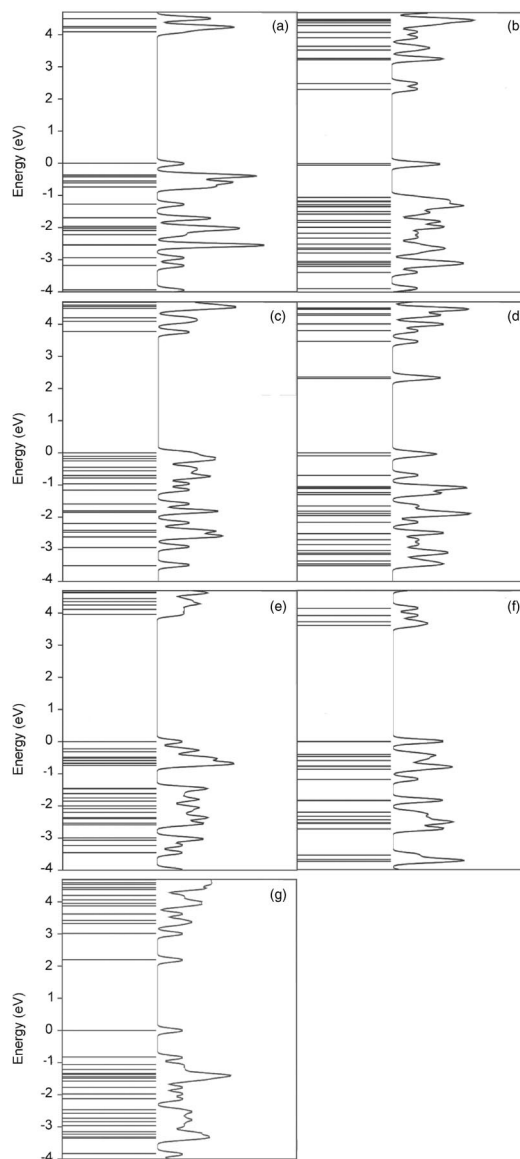


FIG. 2. Energy levels at k -point Γ and total density of states for two fully hydrogenated clusters, $\text{Si}_{14}\text{H}_{20}$ (a) and $\text{Si}_{12}\text{H}_{16}$ (c); for two clusters with Si=O bonds, $\text{Si}_{14}\text{H}_{16}\text{=O}_2$ (b) and $\text{Si}_{12}\text{H}_{16}\text{=O}_2$ (d); for two clusters with Si-O-Si bonds, $\text{Si}_{14}\text{H}_{20}\text{-O}_2$ (e) and $\text{Si}_{12}\text{H}_{16}\text{-O}_2$ (f); for a cluster with one Si-O-Si and one Si=O bond, $\text{Si}_{13}\text{H}_{16}\text{-O=O}$ (g). The zero in each plot refers to the top of the valence band (no relative alignment of the levels has been performed). The direct comparison clearly shows that a strong energy gap reduction, due to the birth of new levels within the hydrogenated energy gap, occurs by adding Si=O bonds at the surface (see also the corresponding values reported in Table II) .

oxidized samples often display an optical gap redshifted with respect to the predicted values³⁹⁻⁴¹ and strong energy differences between absorption and emission peaks position. Attempts which include the Stokes shift between ground and excited states⁴² or take into account the excitonic exchange splitting⁴³ have not been able to overcome the great discrepancy between theory and these experiments. This has suggested that other effects have to be considered. In 1999 some experimental data have provided strong evidences that in

TABLE II. HOMO-LUMO energy gaps (E_g) of the Si_{14^-} , Si_{13^-} , and Si_{12} -core-based clusters.

Structure	E_g (eV)
$\text{Si}_{14}\text{H}_{20}$	4.1
$\text{Si}_{14}\text{H}_{20}-\text{O}_2$	4.0
$\text{Si}_{14}\text{H}_{18}=\text{O}$	2.4
$\text{Si}_{14}\text{H}_{16}=\text{O}_2$	2.3
$\text{Si}_{14}\text{H}_8=\text{O}_6$	2.1
$\text{Si}_{13}\text{H}_{18}-\text{O}$	3.7
$\text{Si}_{13}\text{H}_{18}=\text{O}$	2.4
$\text{Si}_{13}\text{H}_{16}-\text{O}=\text{O}$	2.2
$\text{Si}_{12}\text{H}_{16}$	3.8
$\text{Si}_{12}\text{H}_{16}-\text{O}_2$	3.6
$\text{Si}_{12}\text{H}_{16}=\text{O}_2$	2.3

silicon nanocrystals exposed to oxygen the chemistry of the surface can produce substantial impact on their optoelectronic properties.⁸ Thus the theoretical approaches have started to take into account oxidation and defects at the surface. But to date only a few *ab initio* calculations have been carried out in this direction.^{9–11,44–48}

In this section we report our results on the structural, electronic, and optical properties of isolated silicon clusters covered by hydrogen and oxygen. Various Si/O bond geometries, coverage levels, and cluster sizes have been considered. A comparison with the experimental outcomes concerning PS and heavily oxidized silicon nanoparticles is attempted. During the discussion we compare the results of the electronic energy gaps to the PL energies of PS samples. Because the emission processes are in general different from the absorption ones, this can be considered a nontotally correct approach. Nevertheless, the study of the emission spectra by DFT calculations is still a very difficult task and the few theoretical works on the emission spectra from silicon nanodots including oxygen^{44,47,48} seem to support our conclusions.

A. Model and structural properties

Five classes of clusters have been considered: one with a mean core diameter of 1.0 nm (Si_{35} -core based), three with a mean core diameter of 0.7 nm (Si_{14^-} , Si_{13^-} , and Si_{12} -core based), and one with a mean core diameter of 0.5 nm (Si_{10} -core based). Two types of Si/O bond geometries have been extensively studied: the Si—O—Si backbond (or bridge) and the silanone-like Si=O bond.⁴⁹ In the backbond geometry, typical of the SiO_2 , we have considered the O atom in between both first and second nearest-neighbor Si atoms; in the silanone-like configuration, where the O atom is double bonded with one Si atom, different initial bond orientations have been attempted in order to achieve, by geometry relaxation, a structure that was the closest to the energy global minimum as possible.

The initial cluster geometries have been obtained starting from a crystalline diamondlike Si core structure (i.e., bulk cut) with a T_d interstitial symmetry and a hydrogen termi-

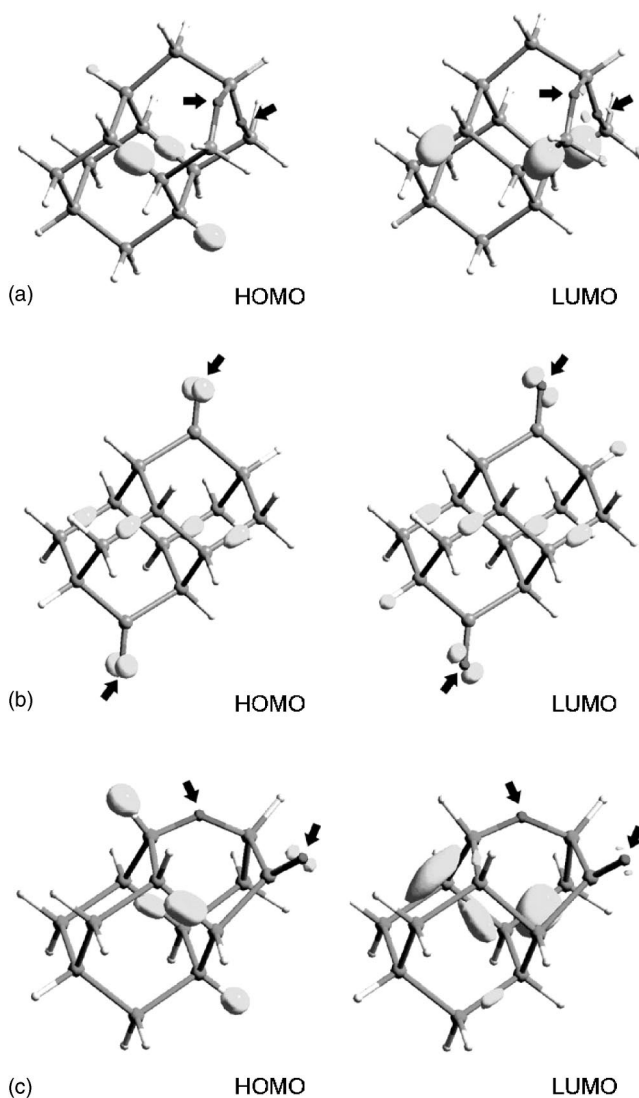


FIG. 3. Comparison of the highest occupied Kohn-Sham orbitals (HOMO's) and the lowest unoccupied Kohn-Sham orbitals (LUMO's) for clusters with three different surface passivation: (a) H and two Si—O—Si bonds, $\text{Si}_{14}\text{H}_{20}-\text{O}_2$; (b) H and two Si=O bonds, $\text{Si}_{14}\text{H}_{16}-\text{O}_2$; (c) H and both types of Si/O bonds, $\text{Si}_{13}\text{H}_{16}-\text{O}=\text{O}$. The isosurfaces at 40% of the maximum amplitude are reported together with the stick and ball representation of the relaxed structures. The black arrows show the location of the oxygen atoms. The localization of the orbitals on the double-bonded oxygen shows clearly that the Si=O bonds strongly influence the character of the states at the band edges also when both types of Si/O bonds are present.

nated surface. The hydrogen atoms are positioned along the tetrahedral directions in order to saturate all the dangling bonds. Because experimental data suggest a crystalline geometry for the Si nanostructures in most of the samples we are interested in (particularly PS), we have considered the crystalline bulk cut as the best starting structure to model the Si core of the clusters. Clusters' geometries obtained by simulated annealing calculations at "high" temperatures can be used as an initial guess if no information about the structural properties of the cluster are available or the simulation

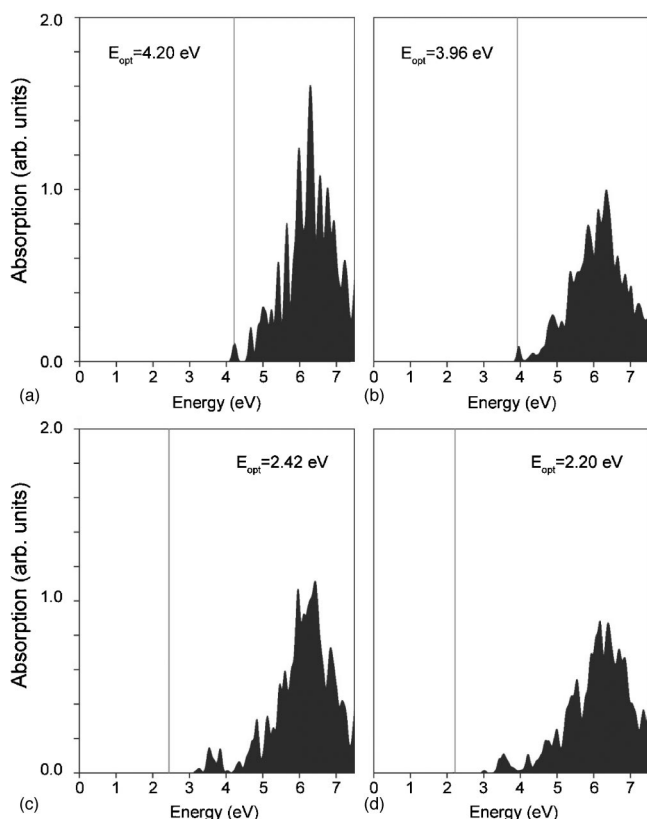


FIG. 4. Calculated absorption spectra for four different Si clusters: (a) $\text{Si}_{14}\text{H}_{20}$, (b) $\text{Si}_{14}\text{H}_{20}-\text{O}_2$, (c) $\text{Si}_{14}\text{H}_{18}=\text{O}$, (d) $\text{Si}_{13}\text{H}_{16}-\text{O}=\text{O}$ (an artificial Gaussian smearing of 0.05 eV has been applied). The optical behavior follows the electronic one with the absorption onset strongly modified by the presence of the $\text{Si}=\text{O}$ double bonds (first optical transitions strongly redshifted).

of a specific formation (growing) procedure is required. Furthermore, the experimental evidences on the “ability” of H to freeze the Si surface in the perfect crystalline geometry, also at room temperature,⁵⁰ support our choice, especially for low oxygen-coverage levels when the dangling bonds at the surface are mainly saturated by H atoms.

The oxidized clusters have been built up substituting H and Si atoms of the initial hydrogen-capped structures with oxygen. In particular the $\text{Si}=\text{O}$ bonds have been obtained by replacing with one oxygen couples of H atoms bonded to the same Si atom. At each oxygen introduction we have studied the different possible configurations of the surface, i.e., different relative locations for the $\text{Si}=\text{O}$ bonds, playing with the symmetry of the systems and the six possible O-double-bond sites available for each cluster. The structures have been then relaxed by total-energy minimization. All the systems, classified by type of Si/O bond and Si-core size, are listed in Table I. The stick and ball representations of some of the final geometries are reported in Fig. 1.

The relaxation has produced structural changes with respect to the initial geometry which strongly depend on the type of surface passivation. A full-H saturation, as expected, leaves unchanged the initial bulklike structure of the Si core. When $\text{Si}=\text{O}$ bonds are added at the surface, the modification of the Si core is very limited. In the relaxed geometry

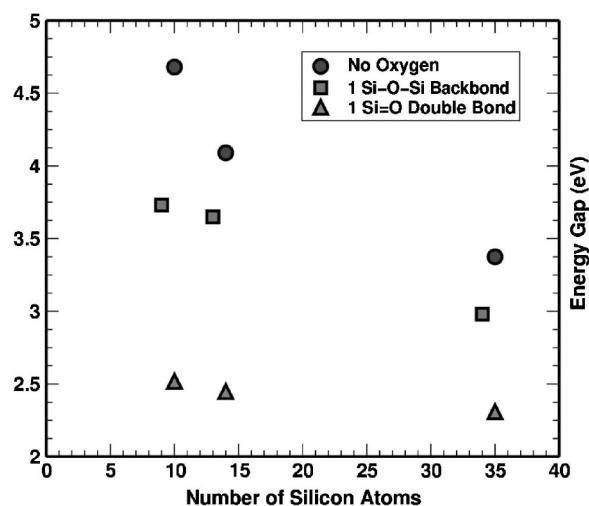


FIG. 5. Energy-gap (E_g) behavior as a function of the number of silicon atoms of the cluster cores, i.e., as a function of the cluster’s size. Circles: full-H passivated surface; squares: with one $\text{Si}-\text{O}-\text{Si}$ bond; triangles: with one $\text{Si}=\text{O}$ bond. While with a full-H passivation the trend follows the quantum confinement theory, with the $\text{Si}=\text{O}$ bond presence the E_g seems practically unaffected by the size of the cluster in agreement with the experimental results of Wolkin *et al.* (Ref. 8).

the $\text{Si}=\text{O}$ bond orientation is always “perpendicular” to the surface, i.e., in the same plane of the two nearest $\text{Si}-\text{Si}$ bonds, along the bisecting line. This final geometry, which does not depend on the number of $\text{Si}=\text{O}$ bonds present at the surface, seems to be supported by an x-ray absorption fine-structure study on the interface between Si and SiO_2 ,⁵¹ which reveals a “strong Si/O bonding oriented preferentially closer to the surface normal.” On the other hand, the introduction of the O atoms in the backbond configuration produces an appreciable modification of the Si core in the vicinity of the bond position, especially when the O are placed in between the first nearest-neighbor Si atoms ($\text{Si}_{14}\text{H}_{20}-\text{O}_2$). The angle and bond-length variations go towards a final geometry for the $\text{Si}-\text{O}-\text{Si}$ close to the quartz one. A more detailed discussion on the structural properties is reported in Ref. 10.

B. Optoelectronic properties: The chemistry of oxygen at the surface

The following discussion is mainly focused on the effects of different Si/O bond geometries at the surface of clusters with the same Si-core size. In particular the results for the three classes of clusters with mean core diameter of 0.7 nm are presented. In addition some results on the effects of the Si-core size on the oxidized clusters are discussed. At the end, a direct comparison with experimental results of Wolkin *et al.*⁸ is attempted.

Once the relaxed geometry has been obtained, the electronic and optical properties of the clusters have been evaluated. In the case of a full-H surface saturation ($\text{Si}_{14}\text{H}_{20}$), a huge opening of the electronic energy gap (E_g) with respect to the Si-bulk case (see Table II) is found, in total agreement

TABLE III. HOMO-LUMO energy-gap values (E_g) for the Si_{10} -, Si_{14} -, and Si_{35} -core-based clusters. All the possible configurations at each oxidation level (number of $\text{Si}=\text{O}$ bonds) are reported. X , Y , and Z label the $\text{Si}=\text{O}$ bond orientation with respect to the system of reference of Fig. 8.

Structure	E_g (eV)
$\text{Si}_{10}\text{H}_{16}$	4.7
$\text{Si}_{10}\text{H}_{14}=\text{O}[Y]$	2.5
$\text{Si}_{10}\text{H}_{14}=\text{O}[Z]$	2.5
$\text{Si}_{10}\text{H}_{12}=\text{O}_2[Z][-Z]$	2.5
$\text{Si}_{10}\text{H}_{12}=\text{O}_2[X][Z]$	2.2
$\text{Si}_{10}\text{H}_{10}=\text{O}_3[-X][-X][Z]$	2.0
$\text{Si}_{10}\text{H}_{10}=\text{O}_3[X][-Y][Z]$	1.6
$\text{Si}_{10}\text{H}_8=\text{O}_4[X][-X][Y][-Y]$	1.9
$\text{Si}_{10}\text{H}_8=\text{O}_4[X][-X][-Y][Z]$	1.7
$\text{Si}_{10}\text{H}_6=\text{O}_5[X][-X][Y][Z][-Z]$	1.7
$\text{Si}_{10}\text{H}_4=\text{O}_6$	1.8
$\text{Si}_{14}\text{H}_{20}$ (FHI98MD)	4.1
$\text{Si}_{14}\text{H}_{18}=\text{O}[Z]$ (FHI98MD)	2.4
$\text{Si}_{14}\text{H}_{18}=\text{O}[Z]$	2.5
$\text{Si}_{14}\text{H}_{16}=\text{O}_2[Z][-Z]$ (FHI98MD)	2.3
$\text{Si}_{14}\text{H}_{16}=\text{O}_2[Z][(x,-y)]$	2.2
$\text{Si}_{14}\text{H}_{14}=\text{O}_3[(x,y)][(x,-y)][Z]$	2.2
$\text{Si}_{14}\text{H}_{12}=\text{O}_4[(x,y)][(x,-y)][(-x,-y)][Z]$	2.1
$\text{Si}_{14}\text{H}_{12}=\text{O}_4[(x,y)][(x,-y)][(-x,y)][(-x,-y)]$	1.9
$\text{Si}_{14}\text{H}_8=\text{O}_6$ (FHI98MD)	2.1
$\text{Si}_{35}\text{H}_{36}$	3.4
$\text{Si}_{35}\text{H}_{34}=\text{O}[Y]$	2.3
$\text{Si}_{35}\text{H}_{32}=\text{O}_2[Y][Z]$	2.2
$\text{Si}_{35}\text{H}_{30}=\text{O}_3[-X][-Y][Z]$	1.8
$\text{Si}_{35}\text{H}_{28}=\text{O}_4[X][-X][Y][-Y]$	1.8
$\text{Si}_{35}\text{H}_{24}=\text{O}_6$	1.7

with the quantum confinement model.⁵ But if hydrogen is replaced by oxygen the situation can change radically. The way the changes occur is strictly related to the Si/O bond type.

With $\text{Si}=\text{O}$ bonds new electronic states appear near both band edges causing a strong reduction (red shift) of the E_g with respect to the full-hydrogen passivation case [Figs. 2(b) and 2(d)]. These new states are mainly localized on the oxygen atoms, as shown by the spatial distribution of the Kohn-Sham orbitals¹⁰ [see, for example, the highest occupied Kohn-Sham orbital (HOMO) and lowest unoccupied Kohn-Sham orbital (LUMO) plotted in Fig. 3(b)]. The more $\text{Si}=\text{O}$ bonds are drawn at the surface the more new oxygen-related states approach the band edges and accumulate there. In this way the electronic and consequently the optical behavior of the clusters become characterized mainly by the double-bonded oxygen. Even the presence of one $\text{Si}=\text{O}$ bond can affect deeply the electronic behavior of the clusters. In the Si_{14} -core-based case, for example, the E_g is reduced by 1.5 eV with the introduction of the first oxygen. This redshift

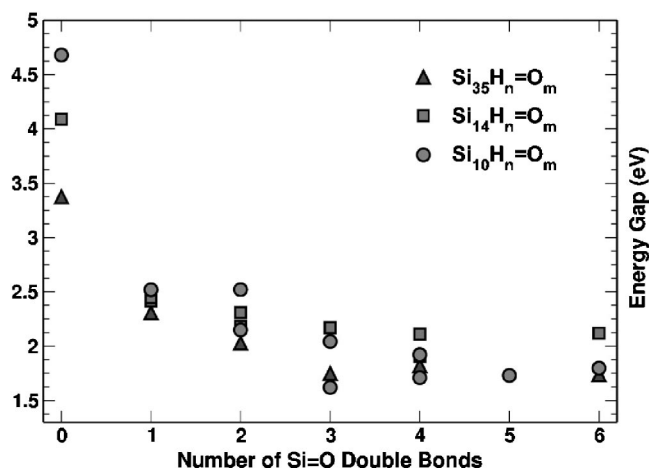


FIG. 6. HOMO-LUMO energy-gap values as a function of the number of $\text{Si}=\text{O}$ bonds at the surface for the three classes of cluster with different core size. Circles: $\text{Si}_{10}\text{H}_n=\text{O}_m$; squares: $\text{Si}_{14}\text{H}_n=\text{O}_m$; and triangles: $\text{Si}_{35}\text{H}_n=\text{O}_m$. The different values for the same cluster at fixed number of $\text{Si}=\text{O}$ bonds correspond to different relative locations of the $\text{Si}=\text{O}$ bonds at the surface. A strong reduction with respect the fully hydrogenated cases occurs with the addition of the first $\text{Si}=\text{O}$ bond. The addition of more $\text{Si}=\text{O}$ bonds produces weaker reductions and a sort of saturation limit seems to be reached.

increases increasing the number of $\text{Si}=\text{O}$ bonds at the surface.

On the other hand, with the addition of $\text{Si}-\text{O}-\text{Si}$ bridges the electronic properties are less affected. The valence band in fact maintains its hydrogenatedlike character and only the conduction-band states show a new weak localization on the added oxygen atoms [Fig. 3(a)]. The E_g is reduced, but not as in the $\text{Si}=\text{O}$ bond cases. Also when the addition of oxygens implies the substitution of some atoms of the Si core, miming the attack of oxygen towards the inner structure, the reduction is still of the order of a few tenths of eV [Fig. 2(f)].

The addition of both types of bonds on the same structure ($\text{Si}_{13}\text{H}_{16}-\text{O}=\text{O}$) produces a final E_g value strongly redshifted [compare Figs. 2(g) and 2(a)], very close to the correspondent results for the double-bond case ($\text{Si}_{13}\text{H}_{18}=\text{O}$). The spatial distribution of the Kohn-Sham orbitals shows an evident localization of the states around the band edges on the oxygen of the $\text{Si}=\text{O}$ bond but not on the $\text{Si}-\text{O}-\text{Si}$ bridge [see the HOMO and LUMO plotted in Fig. 3(c)]. Therefore the electronic properties are mainly related with the presence of the $\text{Si}=\text{O}$ bond which overwhelms the back-bond type. This result is important with respect to the observations of Chabal and co-workers.^{17,52} Studying the initial stage of oxidation of hydrogenated silicon surfaces, they have demonstrated that whereas for the $\text{Si}(111)$ surfaces oxygen is incorporated into $\text{Si}-\text{Si}$ bonds, for the $\text{Si}(100)$ surfaces the initial oxidation involves both the presence of double bonded oxygen and oxygen in the backbond. Yet a cluster contains more or less all the possible surface orientations, thus it is the presence of double-bonded oxygen that mainly determines the electronic and optical properties of the silicon nanoclusters.

The results of the optical properties reflect the electronic ones. In Fig. 4 we show as an example the absorption spectra

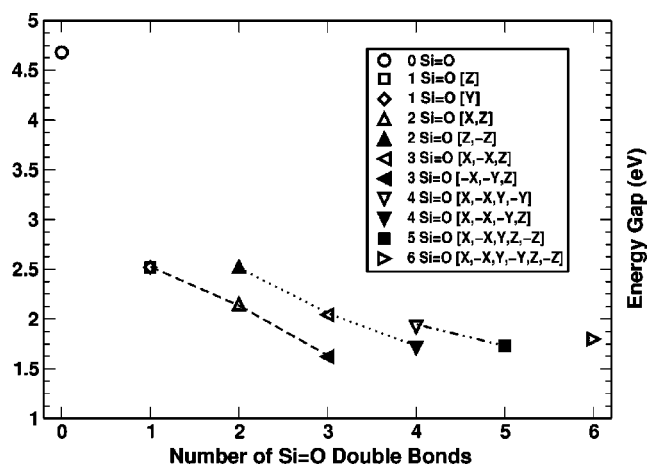


FIG. 7. Energy-gap (E_g) values as a function of the number of Si=O bonds at the surface for the $Si_{10}H_n=O_m$. Each E_g value, which correspond to a specific location of the Si=O bonds, is indicated with a different symbol. The dashed, dotted, and dashed-dotted lines are only guides for the eye and show the further reductions of the E_g when new extra Si=O bonds are added in such a way that the symmetry of the system is reduced.

of some of the clusters (an artificial Gaussian broadening of 0.05 eV has been applied). The huge reduction of the electronic E_g caused by the presence of double-bonded oxygen has its equivalent in the strong redshift of the absorption onset [compare Figs. 4(a) and 4(c)], whereas oxygen in the backbond geometry slightly modifies the absorption behavior [Fig. 4(b)]. With the contemporary presence of oxygen in the double and single bond configuration [Fig. 4(d)] the absorption onset is set exactly at the energy of the transition between HOMO and LUMO (which are Si=O related states) showing that the first optical transitions in this case are mainly due to the Si=O presence. In general it emerges that for all the oxidized clusters the absorption onsets correspond exactly to the HOMO-LUMO transition. Because we find that all the transitions between the near-band-edges states are allowed, the character of those states directly influences the optical activity.

In the previous discussion we have shown that on clusters with the same size the effects of the addition of oxygen atoms strongly depend on the type of Si/O bond that is formed, i.e., on the chemistry of the surface. In Fig. 5 we report the results on the effects of the oxidation once the dimension of the Si core changes. The HOMO-LUMO E_g for three different surface passivations is plotted as a function of the number of the Si-core atoms, i.e., of the cluster size. With a full-hydrogen passivation (circles in Fig. 5) an inverse dependence of the E_g value from the size of the system is displayed, in agreement with the quantum confinement theory. Adding an oxygen in the backbond geometry (squares in Fig. 5) produces a weak reduction of the E_g but still the difference between the values at different sizes is large. With one Si=O bond at the surface instead the E_g seems practically unaffected by the core size: the values (triangles in Fig. 5) lie in fact within less than 0.2 eV. The quantum confinement theory alone fails in explaining this behavior. If the E_g redshift is evaluated as the difference between the full-

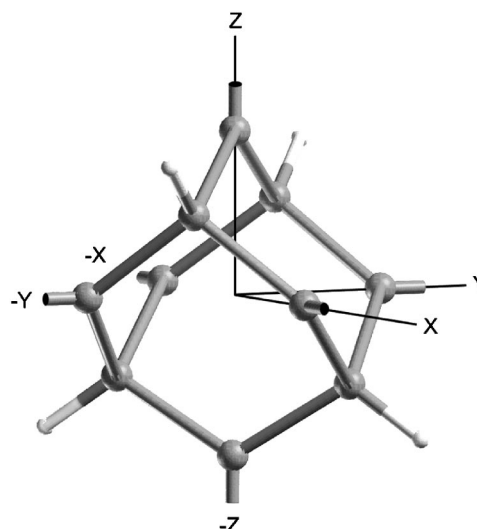


FIG. 8. Cartesian system of reference used to label the different configurations achieved positioning the Si=O bonds on the six available sites. The available sites are indicated as the dangling bonds in the stick and ball representation of the Si_{10} -core class.

hydrogen case and the oxidized one, an inverse dependence of the redshift on the cluster size is displayed.

The experimental results of Wolkin *et al.*,⁸ on the PL behavior of freshly etched PS samples made of crystallites of various sizes, show a large PL redshift when they are exposed to open air. The great amount of the reduction is achieved yet in the few first seconds of exposure⁸ when the oxidation has just begun and it is supposed that only a few O atoms have attacked the surface. This means that our hydrogenated clusters with some Si-H bonds replaced by Si/O bonds can be a reasonable model for this type of samples at the beginning of the exposure. The reported PL shift displays a clear inverse dependence on the initial hydrogenated Si nanocrystallites sizes, the same trend shown by our cluster in the presence of Si=O bonds. Moreover, it is shown that the shift is of the order of 1 eV for samples composed of crystallites smaller than 2 nm in size. If we consider that the size of our clusters is less than a half of the smallest samples of Ref. 8 the agreement between our models with double-bonded oxygen atoms and the experiment is very good. At longer exposure times one can expect that the oxygen attacks the Si structures forming a sort of thin capping SiO_2 . Wolkin *et al.* clearly measure (by Fourier transform infrared spectroscopy) the growing of the signal relative to the presence of the Si/O bonds with the exposure time, which at a certain point saturate indicating a stable situation of the crystallites surface.⁸ In the $Si_{13}H_{16}-O=O$ case, in a certain sense, we model this final situation with the contemporary presence of bridges, typical of the SiO_2 , and Si=O bonds. The new states at the band edges localized on the Si=O bond suggests that also at long times of exposure the predominant role on the optical activity of the nanocrystallites can be played by the Si=O bonds. Therefore in our opinion among the possible configurations for the surface oxidation of silicon crystallites, a model which contains Si=O bonds is the most appropriate to explain the peculiar PL properties of oxidized PS samples and nanocrystals.

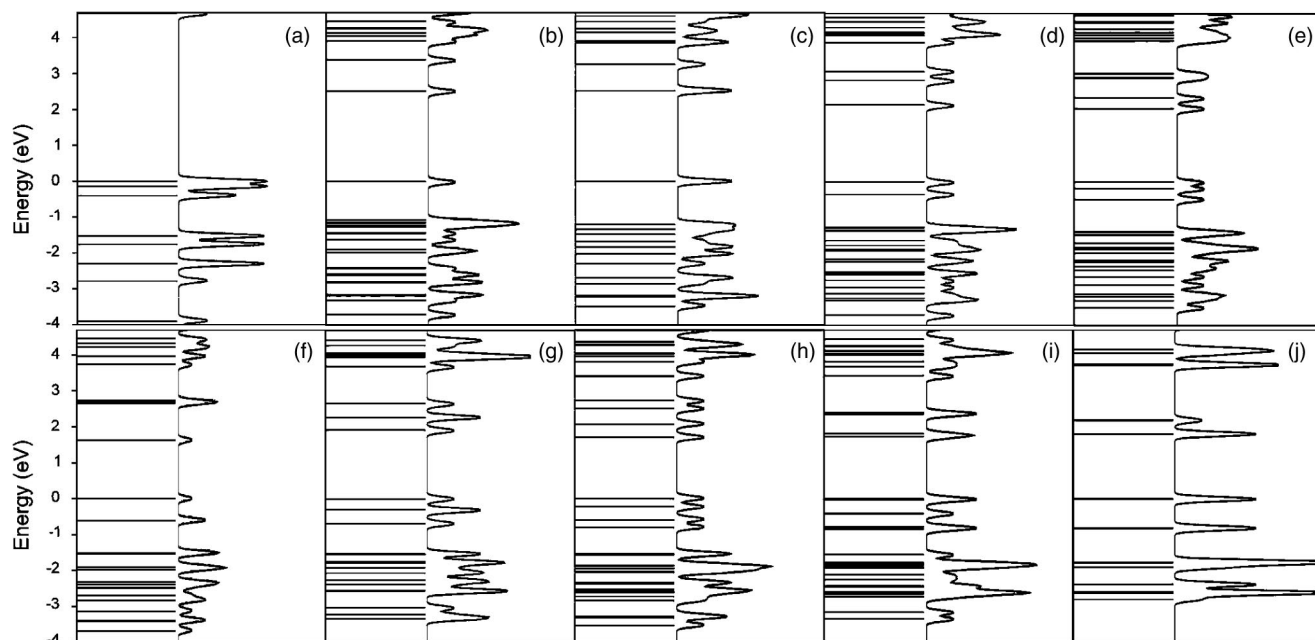


FIG. 9. Energy levels at k -point Γ and total density of states for six different surface configurations of the $\text{Si}_{10}\text{H}_m=\text{O}_n$ class of clusters. (a) $\text{Si}_{10}\text{H}_{16}$; (b) $\text{Si}_{10}\text{H}_{14}=\text{O}[\text{Y}]$; (c) $\text{Si}_{10}\text{H}_{12}=\text{O}_2[\text{Z}][-\text{Z}]$; (d) $\text{Si}_{10}\text{H}_{12}=\text{O}_2[\text{X}][\text{Z}]$; (e) $\text{Si}_{10}\text{H}_{10}=\text{O}_3[\text{X}][-\text{X}][\text{Z}]$; (f) $\text{Si}_{10}\text{H}_{10}=\text{O}_3[-\text{X}][-\text{Y}][\text{Z}]$; (g) $\text{Si}_{10}\text{H}_8=\text{O}_4[\text{X}][-\text{X}][\text{Y}][-\text{Y}]$; (h) $\text{Si}_{10}\text{H}_8=\text{O}_4[\text{X}][-\text{X}][-\text{Y}][\text{Z}]$; (i) $\text{Si}_{10}\text{H}_6=\text{O}_5$; (j) $\text{Si}_{10}\text{H}_4=\text{O}_6$. The zero in each plot refers to the top of the valence band (no relative alignment of the levels has been performed). It is clear that when the $\text{Si}=\text{O}$ bonds are drawn on equivalent “sites” degenerate states appear within the hydrogenated E_g while if they are set on nonequivalent sites the degeneracy is broken causing a higher E_g redshift (compare, for example, the (c) and (d) cases).

C. Optoelectronic properties: Effects of multiple passivation by $\text{Si}=\text{O}$ bonds

In the following we discuss in more detail the results on multiple passivation by $\text{Si}=\text{O}$ bonds. In order to ideally simulate the air exposure of the crystallites in PS samples,⁸ the number of oxygen atoms in the $\text{Si}=\text{O}$ geometry has been progressively increased at the cluster’s surface.

In Table III the calculated electronic gap values are reported for all the core sizes, coverage levels, and different symmetries. As shown before, the E_g with one $\text{Si}=\text{O}$ bond at the surface is set almost at the same value for all the classes of clusters (within 0.2 eV). The addition of new $\text{Si}=\text{O}$ bonds reduces the E_g , but the reduction is not linear with the number of oxygen atoms. In all the cases in fact the strongest redshift is achieved with the first $\text{Si}=\text{O}$ bond. The presence of a second $\text{Si}=\text{O}$ bond produces a further reduction but weaker than the first and so on reaching a sort of saturation limit. This behavior is clearly shown in Fig. 6 where the E_g for the different core sizes is plotted as a function of the number of $\text{Si}=\text{O}$ bonds. Similar calculations performed on a cluster with 66 Si atoms⁵³ confirm our results: the E_g shows a huge reduction with the first four oxygen atoms (in that case 24 sites are available for the formation of $\text{Si}=\text{O}$ bonds) and then a saturation limit occurs.

The addition of new $\text{Si}=\text{O}$ bonds can be done in various ways. For a fixed cluster size and at fixed number of $\text{Si}=\text{O}$ bonds, the different E_g values displayed in Fig. 6 correspond to the various nonequivalent surface configurations achievable. In Fig. 7 the E_g of one class only (Si_{10} -core based) are reported using a different symbol for each of the ten possible

configurations. With one $\text{Si}=\text{O}$ bond the E_g is independent of the site where the bond is formed (compare $\text{Si}_{10}\text{H}_{14}=\text{O}[\text{X}]$ and $\text{Si}_{10}\text{H}_{14}=\text{O}[\text{Y}]$; the adopted Cartesian system of reference is defined in Fig. 8). With two $\text{Si}=\text{O}$ bonds, two types of configuration can be achieved: a more symmetric one, with the two bonds along the same axis (for example $\text{Si}_{10}\text{H}_{12}=\text{O}_2[\text{X}][-\text{Z}]$) and an asymmetric one, with the bonds along different Cartesian axes (for example, $\text{Si}_{10}\text{H}_{12}=\text{O}_2[\text{X}][\text{Y}]$). In the first case the gap is unchanged with respect to the case with one $\text{Si}=\text{O}$ bond, while in the second case a further reduction (around 0.4 eV) occurs. With three $\text{Si}=\text{O}$ bonds we obtain a similar result. Adding a new $\text{Si}=\text{O}$ bond along an axis different from those of the existing $\text{Si}=\text{O}$ bonds induces a further redshift (around 0.5 eV, see the differences between $\text{Si}_{10}\text{H}_{10}=\text{O}_3[\text{X}][-\text{X}][\text{Z}]$ and $\text{Si}_{10}\text{H}_{12}=\text{O}_2[\text{Z}][-\text{Z}]$ and between $\text{Si}_{10}\text{H}_{10}=\text{O}_3[\text{X}][\text{Y}][\text{Z}]$ and $\text{Si}_{10}\text{H}_{12}=\text{O}_2[\text{X}][\text{Z}]$); instead a very small or almost zero reduction of the E_g occurs when the third $\text{Si}=\text{O}$ bond is added along the same axis of an existing $\text{Si}=\text{O}$ bond (see $\text{Si}_{10}\text{H}_{12}=\text{O}_2[\text{X}][\text{Z}]$ and $\text{Si}_{10}\text{H}_{10}=\text{O}_3[\text{X}][-\text{X}][\text{Z}]$). Therefore the introduction of a new $\text{Si}=\text{O}$ bond causes a further reduction of the E_g only if it lowers the symmetry of the system while if the symmetry is maintained the gap remains unvaried. This is explained by the fact that when a new $\text{Si}=\text{O}$ bond is formed at the surface, if its orientation is equivalent to an existing $\text{Si}=\text{O}$ bond, the band-edge states associated with the new bond have the same energy of those of the equivalent pre-existing bond; this brings to a two-times degenerate state at both band edges and no changes in the energy gap [compare, for example, Figs. 9(b) and 9(c)]. If the new bond is formed along a different direction no

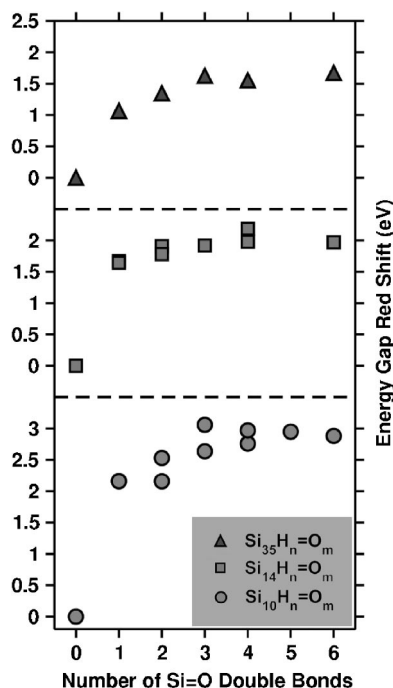


FIG. 10. Energy-gap redshift for three different classes of clusters as a function of the number of Si=O bonds at the surface. Circles: Si₁₀H_n=O_m; squares: Si₁₄H_n=O_m and triangles: Si₃₅H_n=O_m. The redshift is calculated as the difference between a specific surface configuration and the corresponding fully hydrogenated one (thus the zero in the plot for each class stands for the nonoxidized case $m=0$). A saturation tendency is clearly displayed in all the three cases reproducing the results of the PL redshift of oxidized crystallites in PS samples measured by Wolkin *et al.* (Ref. 8).

degeneracy occurs and the new energy levels are shifted in energy with respect to the existing ones with a consequent reduction of the gap [see Fig. 9(d)]. Once the maximum disorder for the surface is reached the addition of further Si=O bonds can produce only an increasing of the symmetry which can lead to an almost null opening of the gaps (see the values for the configurations with four, five, and six Si=O bonds in Fig. 7). A very similar behavior is displayed also by the other classes of clusters, even if the differences between the various configurations become weaker.

Another way of seeing the E_g behavior as a function of the Si=O bond number is to plot the relative redshift with respect to the full-H E_g as done in Fig. 10. The zeros corresponds to the full-H case. A bigger number of Si=O bonds can be seen as a longer exposure to air, i.e., oxidation, of the crystallites in PS samples. Thus, assuming that the excited state does not change radically the band-edges situation at the ground state, the behavior of the E_g redshift as a function of Si=O bonds of Fig. 10 reproduces very closely the behavior of PS samples redshift vs air exposure time of Ref. 8. At the same time Fig. 6 shows clearly how, independently from the size of the clusters, the gaps for oxygen saturated surfaces (six Si=O bonds) assume very similar values, in full agreement with the alignment of the PL peaks measured on oxidized crystallites with different sizes in Ref. 8. The model with multiple Si=O bonds at the surface reproduces

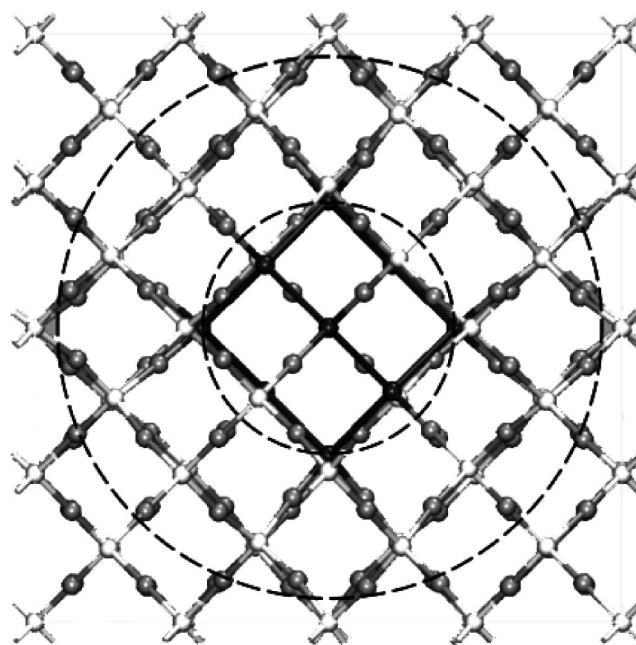


FIG. 11. Top view of the relaxed structure for the Si₁₀/SiO₂ β supercell. The white and the gray balls stand for the Si and O atoms of SiO₂ β , the black ones for the Si atoms of the NC. The two dashed circles help to highlight the three different regions in which the final relaxed structure is organized: the strained Si NC (inner region), a cap shell of distorted SiO₂ β around the NC (between the dashed circles), and an outer region of crystalline SiO₂ β .

amazingly well the experimental outcomes on the optical behavior of intentionally oxidized crystallites in PS samples.^{8,46}

The presence of a saturation limit for the PL redshift can be explained through our model thinking that each Si=O bond acts separately from the others producing its own localized states that interacts very weakly with those produced by another Si=O bond. This view is supported by the comparison of the energy levels and TDOS (as an example, see Fig. 9). Independently from the structure size, for one Si=O bond we see one new state at the top of the VB and one at the bottom of the CB. For two Si=O bonds in the asymmetric case we clearly distinguish two states at the top of the VB and two at the bottom of the VB. For four and six they become four and six, taking into account the degeneracy induced by equivalent Si=O bond positions.

These results can provide a reliable model to explain recent measurements on the PL peak widths of single oxidized silicon quantum dots. Normally, in PS and Si nanocrystal samples, a large PL bandwidth is observed, but this fact can be associated to the presence of silicon nanostructures with different dimensions in the samples. The differences in size bring to different PL energies as a consequence of the quantum confinement effects. Yet Valenta and co-workers⁵⁴ have been able to measure the PL bandwidth of single oxidized Si quantum dots. The Si nanocrystals were fabricated using electron-beam lithography and reactive ion etching resulting in Si nanopillars that were subsequently oxidized to produced luminescent silicon cores. These nanocrystals are organized in a regular matrix which enables repeated observa-

tion of a specific single nanocrystal. Contrary to the expectations a quite large bandwidth (120–210 meV) is observed. This fact is still under debate. Several explanations are possible: the broadening of the PL spectrum could be originated by the participation of one or more phonons to the optical transitions or by the presence of vibrations at the Si nanocluster-SiO₂ interface, or also by the presence of stress in the Si nanocluster core. Our results suggest, however, as a possible explanation, the existence of several localized levels in one single Si nanocrystal due to multiple Si=O bond presence at the surface of the clusters. These levels (see Fig. 9) are separated by about 20–100 meV and can participate to the emission properties of the nanoclusters. At room temperature these levels can be grouped into two broad bands which can be involved in the optical transitions. Thus the width of these bands can be at the origin of the broadened PL. We expect that at lower temperatures the PL broadening will be strongly reduced.

IV. EMBEDDED NANOCRYSTALS

The possibility of a silicon based laser suggested by the optical gain measurements on Si nanocrystals (NC's) formed by ion implantation¹³ and by PECVD (Ref. 14) in SiO₂ has attracted a lot of interest on this type of system and produced a lot of debates especially on the gain mechanisms.¹⁶ Interface states localized at the surface of the light emitting silicon nanocrystals have been proposed as good candidates for explaining the peculiar optical behavior observed.^{13,14} Thus the nature and the properties of the interface between the Si NC and the SiO₂ host matrix has become crucial in order to confirm or not this model. Until the year 2003 the works related to Si clusters or nanocrystals in the presence of oxygen have been all focused on isolated systems (see previous section), except a DFT study on the electronic and optical properties of Si and Ge dots inside a SiC host matrix, in which the authors carried out electronic energy minimization at fixed geometry without performing any structural relaxation.⁵⁵ In 2003 we have published theoretical *ab initio* calculations on small silicon nanocrystals embedded in a SiO₂ matrix.²⁵ It is the first *ab initio* study in which both the host matrix and the embedded nanostructure have been fully relaxed, but it represents only the first step towards more complicated models closer to the real samples. Despite this it can provide fundamental indications on which directions the future calculations have to be pointed and a lot of interesting links to the experimental outcomes have been found.²⁵ In this part of the paper we would like to discuss in more detail all the results not yet presented on this system, in order to give further support to our conclusions regarding the role of the interface region.²⁵ The idea is to present, together with the first part of this paper, a unified discussion on the electronic and optical properties of oxidized silicon nanostructures.

A. Model and structural properties

In the following the main characteristics of the model that has been adopted are summarized. A more detailed description can be found in Ref. 25.

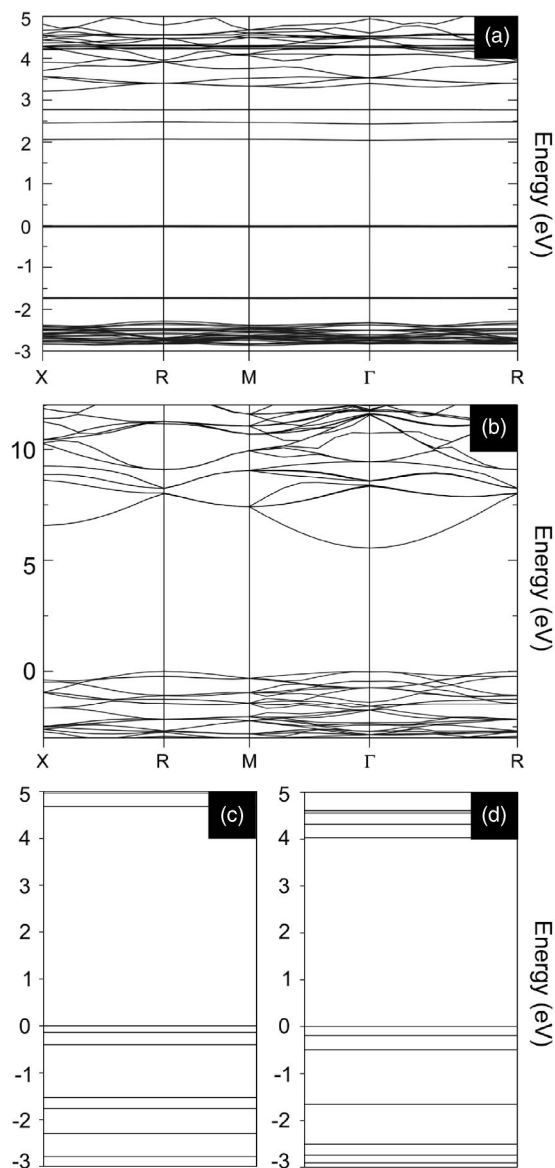


FIG. 12. (a) Electronic band structure along high-symmetry k points of the BZ for the relaxed Si₁₀/SiO₂ β . The zero refers to the top of the valence band. The flat states at the band edges are related to the embedded NC while the dispersed states deep inside the bands show the typical behavior of the SiO₂ β bulk. (b) Electronic band structure along high symmetry k points of the BZ for the pure SiO₂ β bulk. (c) Energy levels at k point Γ for the isolated Si₁₀-NC capped by hydrogen Si₁₀H₁₆(1) at optimized geometry; (d) energy levels at k point Γ for the isolated Si₁₀-NC capped by hydrogen Si₁₀H₁₆(2) with the same Si skeleton of the NC in the relaxed Si₁₀/SiO₂ β [Si-Si bond length 14% strained with respect to the Si₁₀H₁₆(1)]. The zero in each plot refers to the top of the valence band.

In real samples, due to the high-temperature annealing used for the preparation, the SiO₂ is present as amorphous silica. Nevertheless, for the structural model of the embedded nanocrystal, a crystalline SiO₂ has been adopted in order to keep the supercell size as small as possible and to exploit the symmetry. With this approximation a final supercell of 180 atoms has been obtained: 116 atoms are oxygen and 64

are silicon. Ten of these 64 Si atoms are bonded together to form a small nanocrystal, the remaining are bonded with oxygen to form a crystalline host matrix of SiO_2 , in the β -cristobalite form ($\text{SiO}_2\beta$), which surrounds the nanocrystal. The NC tetrahedral coordination is ensured by the peculiar symmetry of the $\text{SiO}_2\beta$. No defects (dangling bonds) are present at the interface and all the O atoms at the NC surface are single bonded with the Si atoms. Unfortunately this geometry implies a high stretching of the Si–Si bond length of the NC with respect to the bulk case (+33%) which has been reduced relaxing the initial supercell by total-energy pseudopotential calculations.

In parallel to the design of the $\text{Si}_{10}/\text{SiO}_2\beta$, we have studied three other systems. The first two are isolated NC's, $\text{Si}_{10}\text{H}_{16}(1)$ and $\text{Si}_{10}\text{H}_{16}(2)$, the third is a pure $\text{SiO}_2\beta$ bulk. The goal is to separate the properties related to the NC from those related to the crystalline matrix in order to check the possible role of the NC/matrix interface. The $\text{Si}_{10}\text{H}_{16}(1)$ and $\text{Si}_{10}\text{H}_{16}(2)$ have been obtained by capping with H atoms the NC taken from the $\text{Si}_{10}/\text{SiO}_2\beta$ structure. For the first one we have extracted the NC from the unrelaxed SiO_2 matrix and relaxed it within a cubic supercell of vacuum ($L=14.32 \text{ \AA}$), with the same prescription used for the $\text{Si}_{10}/\text{SiO}_2\beta$ (same pseudopotentials and XC functional). In the second case the NC core has been taken directly from the relaxed $\text{Si}_{10}/\text{SiO}_2\beta$ geometry, without performing any further relaxation. The comparison between the $\text{Si}_{10}\text{H}_{16}(1)$ and the $\text{Si}_{10}/\text{SiO}_2\beta$ represents a way to understand the $\text{SiO}_2\beta$ matrix influence on the NC relaxation process. The comparison between the isolated NC's, instead, can point out the effects of a strained Si-core structure on the final properties.

From the analysis of the relaxed $\text{Si}_{10}/\text{SiO}_2\beta$ supercell emerges a three-region picture (see the detailed description in Ref. 25): (i) a Si-NC with a strained structure with respect to the bulk Si (but with the strain strongly reduced with respect to the starting geometry), (ii) a cap shell, with a thickness of 8–9 \AA , of distorted $\text{SiO}_2\beta$ which surrounds the NC, progressively reducing its stress going from the NC to

TABLE IV. Energy gaps (E_g) of the $\text{Si}_{10}/\text{SiO}_2\beta$ compared to the $\text{SiO}_2\beta$ bulk and to the isolated NC's. The labels (dir) and (ind) indicates the nature of the gap, respectively direct and indirect.

Structure	GGA-PBE E_g (eV)	LDA E_g (eV)
$\text{Si}_{10}/\text{SiO}_2\beta$	2.1 (dir)	2.0 (dir)
$\text{SiO}_2\beta$ bulk	5.8 (ind)	5.5 (ind)
$\text{Si}_{10}\text{H}_{16}(1)$		4.7 (dir)
$\text{Si}_{10}\text{H}_{16}(2)$		4.0 (dir)

the external region, and (iii) an unstressed crystalline $\text{SiO}_2\beta$ around the shell. These three regions are highlighted in Fig. 11. Despite the simplicity of the model this picture is in close agreement with what emerges from energy-filtered transmission electron microscopy (EFTMEM) and x-ray measurements on Si nanocrystals in SiO_2 samples produced by PECVD.^{25,56} Our result is very important because it provides theoretical information on the structural properties of these types of materials, suggesting the existence of a not-sharp interface between Si NC's and the host SiO_2 matrix in which they are immersed. The SR of the $\text{Si}_{10}\text{H}_{16}(1)$ shows a final crystalline geometry with Si–Si distance very close to the bulk-cut situation. This means that in the embedded case the SiO_2 matrix has highly conditioned the relaxing process of the NC, forcing the bond lengths of the Si skeleton to a mean value between the Si–Si distances in the $\text{SiO}_2\beta$ and the Si-bulk bond length. On the other hand, the presence of the NC has modified the structure of the matrix forcing a rearrangement in its neighborhoods. The system is a whole, in which each part influences the others and cannot be separated from them.

B. Electronic and optical properties

The electronic and optical properties of the relaxed structures of $\text{Si}_{10}/\text{SiO}_2\beta$, $\text{Si}_{10}\text{H}_{16}(1)$, $\text{Si}_{10}\text{H}_{16}(2)$, and $\text{SiO}_2\beta$ bulk have been computed. Figure 12 shows the comparison be-

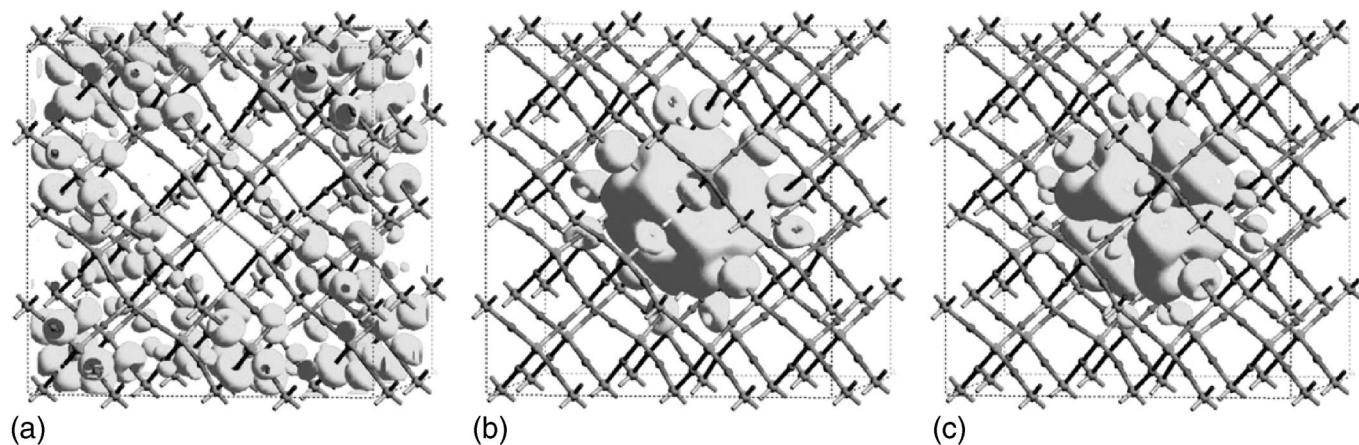


FIG. 13. Isosurfaces (10% of the maximum amplitude) of the square modulus of some of the Kohn-Sham orbitals of the relaxed $\text{Si}_{10}/\text{SiO}_2\beta$ in the valence and conduction bands: (a) HOMO-7; (b) three times degenerate HOMO, HOMO-1, HOMO-2; (c) three times degenerate LUMO, LUMO+1, LUMO+2. Close to the band edges (b) and (c) the orbitals are localized mainly on the NC Si core and partially on the O atoms at the NC/matrix interface [flat, confined states in Fig. 12(a)], while far from the band edges (a) the localization is practically only on the crystalline $\text{SiO}_2\beta$ -bulk part [dispersed states in Fig. 12(a)].

tween the band structures (energy levels) of all the systems. In Table IV the E_g values are reported according to the different levels of theory used in the calculations.

We have also calculated the optoelectronic properties of the $\text{Si}_{10}/\text{SiO}_2\beta$ at the initial geometry (no relaxation). The electronic band structure reveals a clear metallic behavior which has no counterpart in the experimental outcomes. A band-structure calculation on a bulk Si with the same strained Si–Si bond length reveals a similar metallic character, indicating that it is the high strain of the Si skeleton responsible for that behavior. This clearly shows the importance of considering a full optimization of the geometry when studying nanostructures embedded into a host matrix and highlights the risk of modeling this type of system simply combining together the embedded and the host parts as if they were independent.

Looking at the properties of the relaxed structures, we find, on one hand, a strong reduction (around 3.5 eV) of the $\text{Si}_{10}/\text{SiO}_2\beta$ E_g with respect to the $\text{SiO}_2\beta$ -bulk case; on the other hand, a strong reduction (around 2.5 eV) of the $\text{Si}_{10}/\text{SiO}_2\beta$ E_g also with respect to the isolated NC $\text{Si}_{10}\text{H}_{16}(1)$. The reduction with respect to the $\text{SiO}_2\beta$ -bulk case is clearly due to the formation at the CB and VB edges of confined, flat, states as displayed in Figs. 12(a) and 12(b). These new states can only be related to the Si NC presence and they are the evidence of the strong influence of the embedded NC on the electronic properties of the host matrix. Deep inside the bands the typical behavior of the $\text{SiO}_2\beta$ bulk is still recognizable, showing how the NC influence tends to vanish far from the band edges. The strong energy variation with respect to the isolated NC $\text{Si}_{10}\text{H}_{16}(1)$, instead, cannot be due only to the effects of the strain (the final relaxed NC skeleton in the $\text{Si}_{10}/\text{SiO}_2\beta$ case is in fact strained with respect to the bulk geometry). The results for the two hydrogenated NC's, in fact, show that a strained Si structure [$\text{Si}_{10}\text{H}_{16}(2)$], like the one in the relaxed $\text{Si}_{10}/\text{SiO}_2\beta$, can cause a reduction of the E_g with respect to the bulklike case [$\text{Si}_{10}\text{H}_{16}(1)$] at the most of around 0.7 eV. This means that the NC cannot be the only cause of the peculiar electronic behavior of the $\text{Si}_{10}/\text{SiO}_2\beta$, but there must be a key contribution of the surrounding host matrix and in particular of the interface between SiO_2 and NC. The strong interplay between the embedded system and the host material is clearly pointed out.

In Fig. 13(b) the square modulus of the HOMO is reported. The spatial distribution is mainly localized on the Si NC region but some weight on the O atoms at the NC/ SiO_2 interface is evident for low percentage of the charge-density maximum value. The degenerate HOMO-1 and HOMO-2 show the same localization of the HOMO. The HOMO-3 and HOMO-4 (degenerate too) are instead localized on the SiO_2 (the square modulus are in fact distributed on all the O atoms of the host matrix). Because the HOMO-3 and HOMO-4 are still associated to very flat bands, i.e., they are not yet pure $\text{SiO}_2\beta$ -bulk-related states, their spatial localization on the oxide is, in our opinion, a clear proof of the strong interplay between the NC and the surrounding matrix, i.e., of the caps-shell presence. When the typical band behavior of the $\text{SiO}_2\beta$ bulk is displayed (HOMO-6 and HOMO-7, localized at -2.259 and -2.311 eV below the top of the valence band)

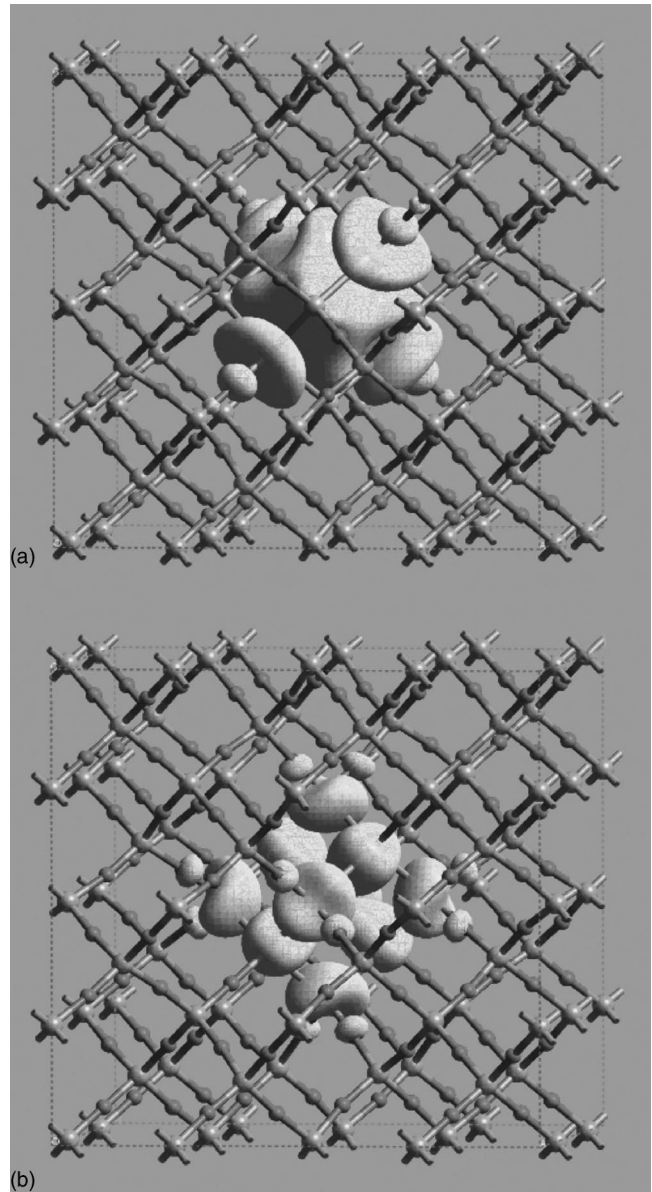


FIG. 14. Isosurfaces at fixed value (10% of maximum amplitude) of the square modulus of the lowest but three (a) and but four (b) unoccupied Kohn-Sham orbitals (LUMO+3 and LUMO+4) for the relaxed $\text{Si}_{10}/\text{SiO}_2\beta$. The tendency of shifting the orbital localization from the Si atoms of the NC core towards the first oxygen atoms around it is clearly displayed.

the orbitals tend instead to be localized on the corner of the supercell [Fig. 13(a)] where the pure crystalline $\text{SiO}_2\beta$ geometry is preserved. This supports our previous conclusion on the organization of the relaxed host matrix. In the CB, the LUMO and the degenerate LUMO+1 and LUMO+2 follow the same trend of the VB top edge. They are localized mostly on the Si NC (but with a different symmetry) and partially on the O atoms at NC/ SiO_2 interface [Fig. 13(c)]. The LUMO+3 loses the Si-NC character and tends to be localized mostly on equivalent oxygen atoms at the NC surface, as witnessed in Fig. 14(a), with a weak contribution on the the NC-nearest-neighbor Si atoms (the same happens for the LUMO+5). LUMO+4 has a NC-centered distribution [Fig.

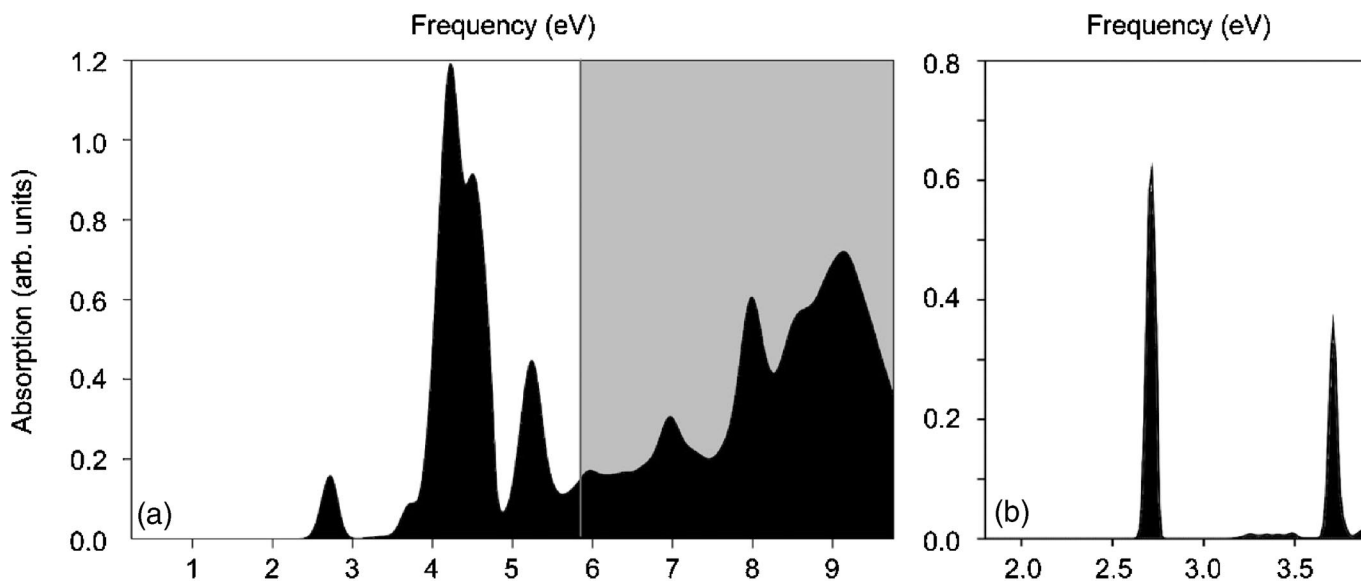


FIG. 15. (a) Absorption spectrum for direct interband transitions between the states of the $\text{Si}_{10}/\text{SiO}_2\beta$ at relaxed geometry (a Gaussian smearing of 0.1 eV has been applied). The gray vertical line indicates the energy onset for the $\text{SiO}_2\beta$ -bulk absorption spectrum. All the features in the white region are not present in the $\text{SiO}_2\beta$ -bulk spectrum and they are related to the presence of the embedded NC. (b) Magnification of the absorption spectrum (a) near the first interesting peak in the onset region (a Gaussian smearing of only 0.02 eV has been applied). The first peak energy corresponds to the transition between the HOMO and the LUMO+3 and/or LUMO+4.

14(b)]. The orbital's localization on the NC supports the view of near-band-edges states related to the NC, suggested by the band-structure analysis; the contribution on the O atoms points out the role of the surrounding SiO_2 on the energy-levels organization. A lot of degenerate NC-related states are present. They reflect the Si_{10} symmetries as the analysis of the $\text{Si}_{10}\text{H}_{16}(1)$ and $\text{Si}_{10}\text{H}_{16}(2)$ energy levels confirm. But despite a general maintenance of the spatial-distribution behavior of the hydrogenated NC's, the NC once embedded in the matrix undergoes a change of the character of its states, with a different organization of the levels near the edges and new contributions on the oxygen atoms both at the interface and partially on the cap-shell structure.

The electronic properties are reflected into the optical ones. Figure 15(a) shows the calculated absorption spectrum for the $\text{Si}_{10}/\text{SiO}_2\beta$ (an artificial Gaussian broadening of 0.1 eV has been applied). The first two peaks, which are set around 2.1 and 2.3 eV, have a very low intensity (not visible in Fig. 15). This means that the associated transitions, $[\text{HOMO}, \text{HOMO}-1, \text{HOMO}-2]/[\text{LUMO}]$ and $[\text{HOMO}, \text{HOMO}-1, \text{HOMO}-2]/[\text{LUMO}+1]$, have a very low probability to occur, i.e., they can be considered forbidden. The first really pronounced feature is centered instead at around 2.7 eV. This energy corresponds to transitions which can involve as initial states the three at the top of the VB, and as final states the LUMO+2, LUMO+3, and LUMO+4. Because the LUMO+2 has the same symmetry of the LUMO+1 and because the transition probability from the top of the VB to the LUMO+1 is very small, we deduce that the transition involving the LUMO+2 is practically forbidden. Thus they remain the LUMO+3 and the LUMO+4. Because the LUMO+3 is mainly localized on the O atoms at the surface of the NC, it follows that the SiO_2 around the NC can directly participate to the optical activity of the system. This

result goes in the same direction of the x-ray experimental outcomes, where through a comparison between total electron yield (TEY) and photoluminescence yield (PLY) it results in an active role in the photoluminescence played by the silica cap shell around the silicon nanocrystals.^{25,56}

The peculiar electronic behavior induced by the NC presence in the $\text{SiO}_2\beta$ supercell produces a new line shape of the absorption onset that results in a completely different optical character with respect to the $\text{SiO}_2\beta$ bulk. New transitions are now displayed in the visible region and at higher energy within the optical gap of the $\text{SiO}_2\beta$ bulk [see in Fig. 15(a) the features on the left of the vertical line which represents the onset of the $\text{SiO}_2\beta$ bulk]. On the other hand, the absorption result for the $\text{Si}_{10}\text{H}_{16}(1)$ displays an onset energy of 4.7–5.0 eV, far away from the values of the $\text{Si}_{10}/\text{SiO}_2\beta$. The $\text{Si}_{10}/\text{SiO}_2\beta$ cannot be reduced to a simple sum of a SiO_2 matrix and an isolated NC. The strong interplay between the silicon nanocrystals and the embedding SiO_2 represents one of the main results of this work. It is an important evidence that has to be taken into account for future characterization of these complicated systems.

V. CONCLUSIONS

In conclusion, we have performed a theoretical study of the properties of Si nanocrystals. We have demonstrated, by first-principle calculations, that the structural, electronic, and optical properties of Si nanocrystals strongly depend on the size and on the different passivation regimes. Starting from hydrogen-covered Si nanoparticles we have shown that single bonded oxygen atoms originate small variations in the electronic properties and bigger changes in the structural properties. On the contrary, oxygen atoms double bonded to silicon make a small contribution to geometry variations, but

a strong reduction in the energy gap. Moreover, when both oxygen types are present at the silicon nanocluster surface, the electronic and optical properties are mainly determined by the oxygen in the double-bond configuration. Thus the presence of double-bonded oxygen atoms seems more appropriate to explain not only the huge redshift observed in photoluminescence, after oxygen exposure, in heavily oxidized silicon nanoparticles,⁸ but also the large photoluminescence bandwidth of single oxidized silicon quantum dots.⁵⁴ In the case of Si nanocrystals embedded in the SiO₂ matrix, our results show that the SiO₂ cage is only slightly deformed by the presence of the nanocrystals, that new electronic states are originated within the silica band gap and that both the Si atoms in the nanocrystals and the O atoms at the interface play a role in the optical properties. This theoretical analysis

clearly point out the important role played not only by the Si nanocrystals but also by a modified silica capping region in determining the optoelectronic properties of the system. Our results help to clarify the experimental outcomes regarding the structural, electronic, and optical properties of Si nanocrystals dispersed in SiO₂.^{25,56,57}

ACKNOWLEDGMENTS

We acknowledge the support of the INFM Advanced Research Project RAMSES, of the INFM National Center for nanoStructures and bioSystems at Surfaces (S³) in Modena and of the MIUR COFIN-PRIN (2002) Italy. All the calculations were performed at CINECA-Bologna and CICAIA-Modena advanced computing facilities.

*Corresponding author. Present address: Theoretical Chemistry Department, Vrije Universiteit, 1081HV Amsterdam, The Netherlands. Email address: luppi@few.vu.nl

- ¹S. Ossicini, L. Pavesi, and F. Priolo, *Light Emitting Silicon for Microphotonics*, Springer Tracts on Modern Physics No. 194 (Springer-Verlag, Berlin, 2003).
- ²*Frontiers of Nano-Optoelectronics Systems*, NATO Science Series II. Mathematics, Physics and Chemistry No. 6 edited by L. Pavesi and E. Buzaneva (Kluwer Academic Publishers, Dordrecht, 2000).
- ³*Silicon Photonics*, Topics in Applied Physics No. 94, edited by L. Pavesi and D. J. Lockwood (Springer-Verlag, Berlin, 2004).
- ⁴L. T. Canham, *Appl. Phys. Lett.* **57**, 1043 (1990).
- ⁵O. Bisi, S. Ossicini, and L. Pavesi, *Surf. Sci. Rep.* **38**, 5 (2000).
- ⁶P. M. Fauchet, in *Silicon Photonics* (Ref. 3), pp. 171–198.
- ⁷R. J. Baierle, M. J. Caldas, E. Molinari, and S. Ossicini, *Solid State Commun.* **102**, 545 (1997).
- ⁸M. V. Wolkin, J. Jorne, P. M. Fauchet, G. Allan, and C. Delerue, *Phys. Rev. Lett.* **82**, 197 (1999).
- ⁹A. Puzder, A. J. Williamson, J. C. Grossman, and G. Galli, *Phys. Rev. Lett.* **88**, 097401 (2002).
- ¹⁰M. Luppi and S. Ossicini, *Phys. Status Solidi A* **197**, 251 (2003).
- ¹¹I. Vasiliev, J. R. Chelikowsky, and R. M. Martin, *Phys. Rev. B* **65**, 121302 (2002).
- ¹²B. Garrido, M. Lopez, O. Gonzalez, A. Perez-Rodriguez, J. R. Morante, and C. Bonafos, *Appl. Phys. Lett.* **77**, 3143 (2000).
- ¹³L. Pavesi, L. D. Negro, C. Mazzoleni, G. Franzò, and F. Priolo, *Nature (London)* **408**, 440 (2000).
- ¹⁴L. D. Negro, M. Cazzanelli, L. Pavesi, S. Ossicini, D. Pacifici, G. Franzò, F. Priolo, and F. Iacona, *Appl. Phys. Lett.* **82**, 4636 (2003).
- ¹⁵J. Ruan, P. M. Fauchet, L. D. Negro, M. Cazzanelli, and L. Pavesi, *Appl. Phys. Lett.* **83**, 5479 (2003).
- ¹⁶*Towards the First Silicon Laser*, Nato Science Series No. 93, edited by L. D. Negro, S. Gaponenko, and L. Pavesi (Kluwer Academic Publishers, Dordrecht, 2003).
- ¹⁷Y. J. Chabal, K. Raghavachari, X. Zhang, and E. Garfunkel, *Phys. Rev. B* **66**, 161315 (2002).
- ¹⁸M. Bockstedte, A. Kley, J. Neugebauer, and M. Scheffler, *Comput. Phys. Commun.* **107**, 187 (1997).
- ¹⁹Cambridge Serial Total Energy Package, Version 4.2.1, 1 October 2000.
- ²⁰V. Milman, B. Winkler, J. A. White, C. J. Pickard, M. C. Payne, E. V. Akhmatkaya, and R. H. Nobes, *Int. J. Quantum Chem.* **77**, 895 (2000).
- ²¹Cerius² Users Guide and Materials Studio 2.1.5 Users Guide for CASTEP, MSI and Accelrys Inc. 2000–2002.
- ²²L. Kleinman and D. M. Bylander, *Phys. Rev. Lett.* **48**, 1425 (1982).
- ²³N. Troullier and J. L. Martins, *Phys. Rev. B* **43**, 1993 (1991).
- ²⁴D. Vanderbilt, *Phys. Rev. B* **41**, R7892 (1990).
- ²⁵N. Daldosso, M. Luppi, S. Ossicini, E. Degoli, R. Magri, G. Dalba, P. Fornasini, R. Grisenti, F. Rocca, L. Pavesi, S. Boninelli, F. Priolo, C. Spinella, and F. Iacona, *Phys. Rev. B* **68**, 085327 (2003).
- ²⁶T. Takagahara and K. Takeda, *Phys. Rev. B* **46**, 15 578 (1992).
- ²⁷D. J. Lockwood, *Solid State Commun.* **92**, 101 (1994).
- ²⁸B. Delley and E. F. Steigmeier, *Phys. Rev. B* **47**, 1397 (1993).
- ²⁹J. P. Proot, C. Delerue, and G. Allan, *Appl. Phys. Lett.* **61**, 1948 (1992).
- ³⁰L. W. Wang and A. Zunger, *J. Phys. Chem.* **98**, 2158 (1994).
- ³¹S. Ogut, J. R. Chelikowsky, and S. G. Louie, *Phys. Rev. Lett.* **79**, 1770 (1997).
- ³²M. Rohlfing and S. G. Louie, *Phys. Rev. Lett.* **80**, 3320 (1998).
- ³³I. Vasiliev, S. Ogut, and J. R. Chelikowsky, *Phys. Rev. Lett.* **86**, 1813 (2001).
- ³⁴C. S. Garoufalis, A. D. Zdetsis, and S. Grimme, *Phys. Rev. Lett.* **87**, 276402 (2001).
- ³⁵J. C. Grossman, M. Rohlfing, L. Mitas, S. G. Louie, and M. L. Cohen, *Phys. Rev. Lett.* **86**, 472 (2001).
- ³⁶H. C. Weissker, J. Furthmüller, and F. Bechstedt, *Phys. Rev. B* **67**, 245304 (2003).
- ³⁷A. Franceschetti and S. T. Pantelides, *Phys. Rev. B* **68**, 033313 (2003).
- ³⁸S. Furukawa and T. Miyasato, *Phys. Rev. B* **38**, 5726 (1988).
- ³⁹S. Schuppler, S. L. Friedman, M. A. Marcus, D. L. Adler, Y. H. Xie, F. M. Ross, T. D. Harris, W. L. Brown, Y. J. Chabal, L. E. Brus, and P. H. Citrin, *Phys. Rev. Lett.* **72**, 2648 (1994).
- ⁴⁰S. Schuppler, S. L. Friedman, M. A. Marcus, D. L. Adler, Y. H. Xie, F. M. Ross, Y. J. Chabal, T. D. Harris, L. E. Brus, W. L.

- Brown, E. E. Chaban, P. F. Szaiewski, S. B. Christman, and P. H. Citrin, *Phys. Rev. B* **52**, 4910 (1995).
- ⁴¹J. von Behren, T. van Buuren, M. Zacharias, E. H. Chimowitz, and P. M. Fauchet, *Solid State Commun.* **105**, 317 (1998).
- ⁴²E. Martin, C. Delerue, G. Allan, and M. Lannoo, *Phys. Rev. B* **50**, 18 258 (1994).
- ⁴³T. Takagahara and K. Takeda, *Phys. Rev. B* **53**, R4205 (1996).
- ⁴⁴M. J. Caldas, *Phys. Status Solidi B* **217**, 641 (2000).
- ⁴⁵M. Luppi and S. Ossicini, *Mater. Sci. Eng., B* **101**, 34 (2003).
- ⁴⁶M. Luppi and S. Ossicini, *J. Appl. Phys.* **94**, 2130 (2003).
- ⁴⁷A. B. Filonov, S. Ossicini, F. Bassani, and F. Arnaudd'Avitaya, *Phys. Rev. B* **65**, 195317 (2002).
- ⁴⁸A. Puzder, A. J. Williamson, J. C. Grossman, and G. Galli, *J. Am. Chem. Soc.* **125**, 2786 (2003).
- ⁴⁹F. Zhou and J. D. Head, *J. Phys. Chem. B* **104**, 9981 (2000).
- ⁵⁰S. Bouzidi, F. Coletti, J. M. Debever, P. A Thiry, P. Dumas, and Y. J. Chabal, *Phys. Rev. B* **45**, 1187 (1992).
- ⁵¹R. Sammynaiken, S. J. Naftel, T. K. Shamb, K. W. Cheah, B. Averboukh, R. Huber, Y. R. Shen, G. G. Qin, Z. C. Ma, and W. H. Zhong, *J. Appl. Phys.* **92**, 3000 (2002).
- ⁵²X. Zhang, Y. J. Chabal, S. B. Christman, E. E. Chaban, and E. Garfunkel, *J. Vac. Sci. Technol. A* **19**, 1725 (2001).
- ⁵³A. Puzder, A. J. Williamson, J. C. Grossman, and G. Galli, *J. Chem. Phys.* **117**, 6721 (2002).
- ⁵⁴J. Valenta, R. Juhasz, and J. Linnros, *Appl. Phys. Lett.* **80**, 1070 (2002).
- ⁵⁵H.-Ch. Weissker, J. Furthmller, and F. Bechstedt, *Phys. Rev. B* **65**, 155327 (2002).
- ⁵⁶N. Daldosso, G. Dalba, R. Grisenti, L. D. Negro, L. Pavesi, F. Rocca, F. Priolo, D. Pacifici, G. Franzò, and F. Iacona, *Physica E (Amsterdam)* **16**, 429 (2003).
- ⁵⁷G. V. Prakash, N. Daldosso, E. Degoli, F. Iacona, M. Cazzanelli, F. Rocca, Z. Gaburro, G. Puker, P. Dalba, E. C. Moreira, G. Franzò, D. Pacifici, F. Priolo, C. Arcangeli, A. B. Filonov, S. Ossicini, and L. Pavesi, *J. Nanosci. Nanotechnol.* **1**, 159 (2001).